CHALMERS
UNIVERSITY OF TECHNOLOGY

Electromechanical Damping of Primary Control Surfaces for an Electric Aircraft

Damping characteristics of an actuator in case of power loss

Master's thesis in Systems, Control and Mechatronics

Alinder Anton
Olsson Oskar

DEPARTMENT OF ELECTRIC ENGINEERING
CHALMERS UNIVERSITY OF TECHNOLOGY
Gothenburg, Sweden 2023
www.chalmers.se

Master's thesis 2023

Electromechanical Damping of Primary Control Surfaces for an Electric Aircraft

Damping characteristics of an actuator in case of power loss

Alinder, Anton
Olsson, Oskar

CHALMERS
UNIVERSITY OF TECHNOLOGY

Department of Electrical engineering
Chalmers University of Technology
Gothenburg, Sweden 2023

Electromechanical Damping of Primary Control Surfaces for an Electric Aircraft
Damping characteristics of an actuator in case of power loss
ANTON ALINDER OSKAR OLSSON

Supervisor: Pond, Welsh, Flight Controls at Heart Aerospace
Examiner: Grauers, Anders, Department of Electrical Engineering at Chalmers

Master's Thesis 2023
Department of Electrical engineering
Systems and control
Chalmers University of Technology
SE-412 96 Gothenburg
Telephone +46 31 772 1000

Cover: Visualization of Heart aerospace aircraft ES-30

Typeset in LaTeX
Printed by Chalmers Reproservice
Gothenburg, Sweden 2023

Abstract

This thesis evaluate a new type of electromechanical actuator's ability to withstand external forces applied to the primary control surfaces of an aircraft, to determine if this actuator design can meet some of the critical requirements. The electromechanical actuator is a new product of an Italian company, UMBRAGROUP. A collaboration with them was carried out to create the simulation environment for the actuator. When the electromechanical actuator suffers from power loss it is crucial that it does not lose all damping performance. Therefore different resistances connected between the phases of the electric motor were investigated in order to induce current. The purpose is to generate a Back-Electromotive Force that will counteract the oscillation in the surface connected to the actuator. Simulations of the electric circuit and the mechanical system in MATLAB and SIMULINK showed that it is possible to damp the movement of a control surface. Furthermore, it was analysed how to affect the actuators bandwidth and how to determine the actuators damping coefficient.

Keywords: Actuator, aviation, damping, electromechanical, electromotive force, flutter, gearing, short circuit.

Acknowledgements

This thesis would not be possible without several important people. First of all we would like to thank the flight controls department at Heart Aerospace and especially Welsh Pond for their patient, knowledge and helpfulness. Secondly a big gratitude against UMBRAGROUP in Foligno Italy for their invaluable help creating the MATLAB model and input during the project.

Lastly we are very grateful for the invaluable input from our supervisor and examinator Anders Grauers for his knowledge, guidance and valuable time.

Anton Alinder
Oskar Olsson

Gothenburg, June 2023

List of Acronyms

Below is the list of acronyms that have been used throughout this thesis listed in alphabetical order:

BEMF	Back electromotive force
EM	Electrical motor
EMA	Electromechanical Actuator
PMSM	Permanent Magnetic Synchronous Motor
RC-circuit	Resistor-Capacitor-circuit

Nomenclature

Below is the nomenclature of parameters that have been used throughout this thesis.

Parameters

If nothing else is stated the following parameters was used:

$R_d = 100 \quad [\Omega]$	Damping circuit resistance
$R_{sf} = 3.3995 \quad [\Omega]$	Resistance of each electric motor coils
$L_{sf} = 0.0139 \quad [H]$	Inductance of each electric motor coils
$Kt = 2.1390 \quad [\frac{Nm}{A_{max}}]$	Electric motor torque constant
$Kef = 1.1140 \quad [\frac{V_{ph,max}s}{rad}]$	Electric motor constant
$PP = 10 \quad [-]$	Number of pole-pairs
V_{ph}	Phase voltage.

Variables

τ	Induced torque [Nm]
T	Applied Torque [Nm]
ω_r	Angular velocity of rotor [rad/s]
ω_{os}	Angular velocity of output shaft [deg/s]
P	Power [W]
Φ	Flux
B	Magnetic flux

Contents

List of Figures

List of Tables

1
Introduction

1.1 Background

In recent years development of electrical aircraft have taken big steps and is now aiming for a near term introduction of commercial electric aircrafts. Weight reduction of the fuselages is crucial in order to reduce cost of the batteries. This enforces the components of the aircraft to be, not only robust and safe, light-weighted compared to the components of a combustion-driven aircraft. The control of the primary control surfaces are often driven by hydraulic actuators [1]. However, for an all electric aircraft it is desired to use electrical actuators. To enable this, the electromechanical actuator (EMA) need to perform as good as or better than a hydraulic actuator in terms of damping ability.

1.2 Objective and scope

The aim of this thesis is to analyse an electromechanical actuator's damping ability on an aircraft's primary control surfaces. A proof of concept to decide whether an electromechanical actuator placed directly on the hinge line is strong enough to provide damping when suffering from power loss. The evaluation of the concept is made through simulations where the actuator is exposed to external forces that represent air load.

1.3 Limitations of the study

The electromechanical actuator used on the aircraft consist of two permanent magnetic brushless AC-motors. To evaluate the actuator's damping performance in a damping mode, it is sufficient to use one motor on a single shaft. Therefore the calculations on the actuator are based on a model where one motor is removed from the EMA. Material stress is not a part of this study. When the actuator suffers power loss it is assumed that there is no component failure, the actuator system is intact but needs to provide damping without any external power source.

1.4 Ethics and data

The simulations for this thesis are created through a Simulink-model developed by UMBRAGROUP. However, the simulation model only use parts that is provided by

Mathworks. No personal data is used, and the results from the simulations do not provide any biased result connected to a specific method.

2

Theory of primary control surfaces systems

In this chapter, the different primary control surfaces are introduced in section 2.1. Furthermore, a traditional solution is presented in section 2.2. Thereafter, information and theory regarding the new electromechanical actuator is presented in section 2.3 to 2.9. Finally the phenomena to prevent flutter is explained in section 2.10, as well as the gust lock in section 2.11.

2.1 Primary control surfaces

The primary control surfaces of an aircraft includes ailerons, elevators and rudder as seen in figure 2.1. These control surfaces are responsible for steering the direction of the aircraft in all 6 degrees of freedom. The ailerons controls the roll angle, the elevators controls the pitch angle and the rudder controls the yaw angle.

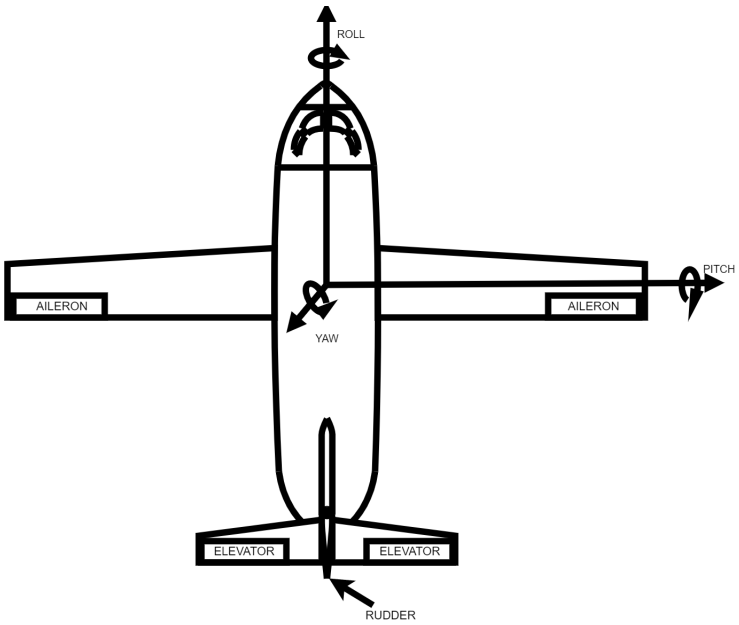

Figure 2.1: Primary control surfaces of an aircraft

The most common way to control the primary control surfaces is with linear hydraulic actuators. This design transform a transitional movement to the desired

rotation as in figure 2.2a. Since the vehicle industry goes towards electrification, a desire to eliminate weight exists. This can be achieved by replacing hydraulic actuators with electromechanical actuators [2]. The alternative to a linear actuator is a rotational actuator, mounted directly to the hinge line as in figure 2.2b. This is the design of the analyzed actuator throughout this thesis. It reduces weight and the number of components such as a rod and lever required for the linear actuator.

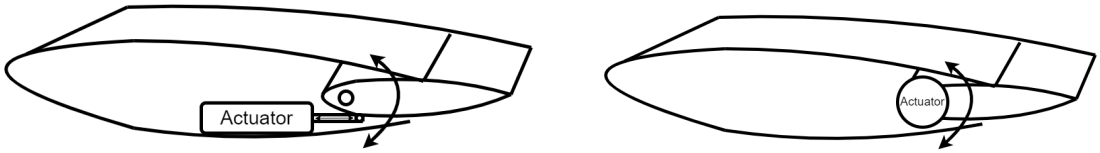

(a) Linear actuator **(b)** Rotational actuator

Figure 2.2: Two different mountings of actuators on an aileron

2.2 Hydraulic actuator

Hydraulic actuators have a fast response time which makes them a good choice when it comes to prevent external disturbances. With no use of electricity in an hydraulic actuator, no electric hazards can occur and therefore the risk of starting a fire is minimal. The main advantage is the ability to handle almost unlimited work due to the great generated force from the actuator. This force is created through hydraulic fluid that is pumped by either an electric or motor driven pump through a selector valve which creates extra pressure. When the fluid reaches the actuator the pressure push a piston forward creating a linear force. The force can be used for flight control systems [3]. If an aircraft suffers problems with the actuator system, the actuator is set to damping mode. This is done by having two chambers containing the oil as in figure 2.3. In the channel between the chambers an orifice plate is placed with holes letting the hydraulic oil flow through slowly. This construction makes it hard to push or pull the shaft creating a damping effect. This is a desired effect as an aircraft can still be operable if the surface stays still or move slowly. The amount of damping is decided by the size of the holes in the orifice plate and the viscosity of the oil [4].

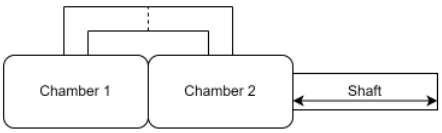

Figure 2.3: Hydraulic actuators chambers

In an aircraft application it is required to have two parallel systems connected to a primary control surface to ensure safety if one system suffer from a failure. Therefore, the ailerons, rudder and elevators requires two separated actuators each. However,

two separated actuators are heavy and therefore other more light-weighted solutions are considered.

2.3 Permanent Magnet Synchronous Motor

The electromechanical actuator is driven by two Permanent Magnet Synchronous Motors (PMSM). Permanent magnets are mounted on the rotor for the creation of the magnetic field, instead of windings. The magnetic field of the stator is created in between the air gaps when exposed to a currents through the windings. The torque is produced when the rotor field poles are holding the magnetic field rotating in a synchronous speed. The torque generated is necessary for the damping ability of the EMA, since the torque shall withstand external forces on the primary surface connected to the EMA [5].

2.4 Elevators

Elevators are located at the rear of the aircraft as in figure 2.1. The elevators are part of the control surfaces designed to control the aircraft's movements together with ailerons and the rudder [6]. The elevators is a crucial surface controlling the pitch of the aircraft, the angle of attack. If the elevators actuation system or the surface itself would to fail it can have a fatal outcome and is therefore the most crucial surface to be able to damp. Therefore this study focus on UMBRAGROUP's actuator damping ability of the elevators. By rotating the elevator upwards the tail is pushed down, nose goes up, and the aircraft's angle of attack changes and the aircraft increase in altitude. Vice versa when rotating the elevator downwards [6].

2.5 Motor Controller Electronic components

The EMA consists of two AC PMSM, with two separated Motor Control Electronics (MCE). It contains some crucial electronic components for the control of the motors such as MOSFETS, H-bridges and a Resistor capacitor circuit.

2.5.1 MOSFET

Metal-oxide-semiconductor field-effect transistor (MOSFET), is a very effective voltage controlled component controlling the current flowing through it. It can be described as a variable resistor, and during a power loss the resistance is very high for the specific actuators MOSFET, almost acting as an open circuit (zero current passing through) [7]. With the voltage applied, the resistance is very low and thereby acting as a short circuit.

2.5.2 H-bridges

An H-bridge consists of four switches that enables the direction of the current to alternate through a component. These switches are usually MOSFETs and these

are arranged in pairs, 2-by-2, 4-by-4 etc. By the help of this mechanism the motor is able to run counter- and clockwise [8]. The H-bridges are the link between the MCE and the EM's and is therefore an important component in the MCE.

2.5.3 Resistor Capacitor circuit

A Resistor Capacitor (RC) circuit consists of a resistance connected with a capacitor, powered by a voltage source. The capacitor can store electric charge, which is useful in ac circuit where the voltage vary as sine waves with different frequencies. RC-circuits can then be used as filters in order to filter out the unwanted noise from the power source [9]. On the contrary, when suffer power loss this will provide some impedance that can affect the behavior of the actuator.

2.6 Electromechanical actuator

The electromechanical actuator (EMA) provided is designed with a dual loaded shaft with two electrical motors attached to it. Further, two output shafts from the same actuator, separated from each other between the output shafts to the MCE's. The aircraft industry have high requirements on safety, in a similar concept as the hydraulic actuators in section 2.2, it is required to have two separated, independent channels. Therefore the system have two separated MCE's that controls one electric motor each. The actuator have two permanent magnet synchronous ac-motors connected to a mechanical gearing without any gearwheels. The EMA provides a high gear ratio through multiple ball-screw-nuts. The main advantages of using this EMA configuration compared to the hydraulic system is the weight reduction. By this dual EM system it is possible to achieve the parallel channels with only one EMA, instead of the two separated actuators required by the hydraulic system. Dual separated actuators also suffers from force-fighting [4]. This is when the separated hydraulic actuators pull or push the surface slightly differently, creating a stress in the material, even while synchronized it can not be neglected. This issue is eliminated by the provided EMA. The actuator need to be able to both rotate freely and oppose the external forces when suffering from a power loss. This to avoid the passive EM acting as a generator and fighting the active EM.

The actautor is powered and controlled by a MCE that receive both 18VDC and 270VDC for low voltage components and power supply to the electric motors. The MCE consists of micro controllers, H-bridges and a RC-circuit as in section 2.5. The Micro controllers is supplied with 18VDC and control the three independent H-bridges by pulse width modulation (PWM) signals. For this thesis the actuator is simplified with one system, one electric motor and a single shaft. However the dual electric motor system is discussed in section 5 of the results from the single electric motor actuator.

2.7 Friction of the actuator

If the EMA from UMBRAGROUP was disconnected from the MCE, in other words nothing is connected to the EM phases, the only opposing force when rotating the output shaft is the internal friction and inertia. In a PMSM this friction comes from the gearing itself of the actuator, Since no brushes create friction. Additionally, air resistance of the rotor in the EM is neglected. Furthermore the size of the gearing in this specific actuator only slightly affect how much force applied on the shaft is required to make it move.

2.8 Short circuit designs

There are different possibilities to short circuit a motor depending on what current and voltage it should generate. The two most common ways in a symmetric three-phase system is Y-Y, figure 2.4, or Delta-Delta connection, figure 2.5. In Y-Y configuration the line voltage is the phase voltage times a factor of $\sqrt{3}$. In an asymmetric three-phase system, for instance Y-Delta or Delta-Y configurations, one need to go through the system in a two-step process. First the line voltage from the generator or the load need to be decided, as well as the current. Then this voltage and current is transitioned from that line to the other line. Another option is the Delta with open terminals configuration as in figure 2.6. In the Delta-Delta configuration the voltage across one load leg, A-B, is equal to the corresponding generator leg, A'-B' in figure 2.4. For the Y-configuration the same principle goes for the current, the current through one load leg equal to the current in the corresponding generator leg. In this case the three phases are shorted independently, from A+ to A-, B+ to B- and C+ to C- [10]. This is advantageous from a physical standpoint as it enables the short circuit design to be implemented inside the H-bridge corresponding to each EM phase.

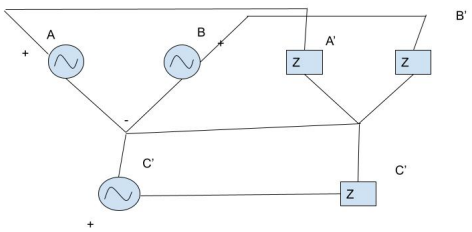

Figure 2.4: Y-Y configuration

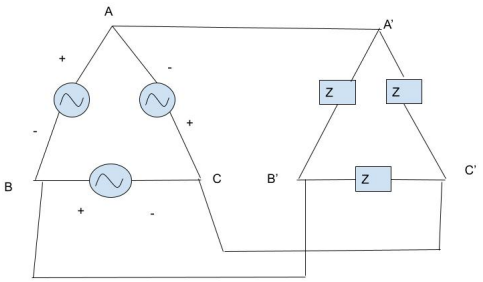

Figure 2.5: Delta-Delta configuration

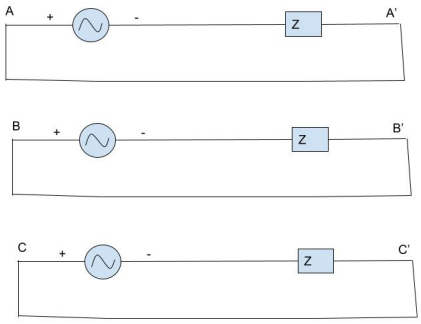

Figure 2.6: Delta-Open configuration

2.9 Electromotive force

Electromotive force, EMF is defined as the "voltage induced due to variation of flux, Φ, through an area enclosed by a conductor loop, and is equal to negative rate of change with time of linked flux" [11]. Given that the magnetic flux that passes through a coil of cross section area is

$$\Phi = BA \tag{2.1}$$

where B is the magnetic flux density and A is the coil of the cross section, the EMF can be written as

$$e = \frac{-d(BA)}{dt} = -A\frac{dB}{dt} - B\frac{dA}{dt}. \tag{2.2}$$

This shows that the EMF can, given a time-variant magnetic field, be induced in a coil. However, for a trapezoidal EMF the induced voltage can be expressed as

$$e = PP\Phi\omega_r \qquad [12] \tag{2.3}$$

Where PP is to pole-pair and ω_r is the angular velocity of the rotor. The important to take from here is that the induced voltage, e, is dependent on ω_r.

2.10 Flutter

Flutter is a physical phenomenon that creates unwanted oscillations and it arise in structures affected by aerodynamic forces [13]. It occurs as a consequence of a relationship between stiffness, aerodynamics and inertial forces on the structure. Flutter is relevant for this study since the purpose is to show the damping ability of the electromechanical actuator, damping that will prevent flutter from occurring. When the wind speed increases to a point the structure is no longer able to damp out the motions caused when the aerodynamic energy hits the surface. The vibration can be extremely dangerous and cause structural damage, therefore flutter prevention is a crucial part of aircraft design.

2.11 Gust Lock

Gust Lock or Flight Control Lock is a device which prevents the aircraft surface from movement that is caused randomly by atmospheric disturbances or gust when the aircraft is powered down. It varies depending on the size of the aircraft and what kind of surface that should be protected [14]. With the new type of actuator applied on the primary surfaces, the desire is to use the EMA as a Gust Lock in order to save the aircraft from additional weight of an external Gust Lock.

3

Methods

For evaluation purposes a model of the actuator is designed for the ES30 aircraft elevator, however the principle is applicable to other electrical actuator models. First in sector 3.1 the actuator layout and the tests needed to find the behaviour is presented. Secondly in section 3.2 the damping circuit design is evaluated to ensure high induced current. Then the systems targets is presented in section 3.3 and lastly the simulation environment is presented in section 3.4.

3.1 Actuator design and tests

In this actuator design, as in figure 3.1 the behaviour of the motor and gearing are investigated as well as the impedance of the MCE.

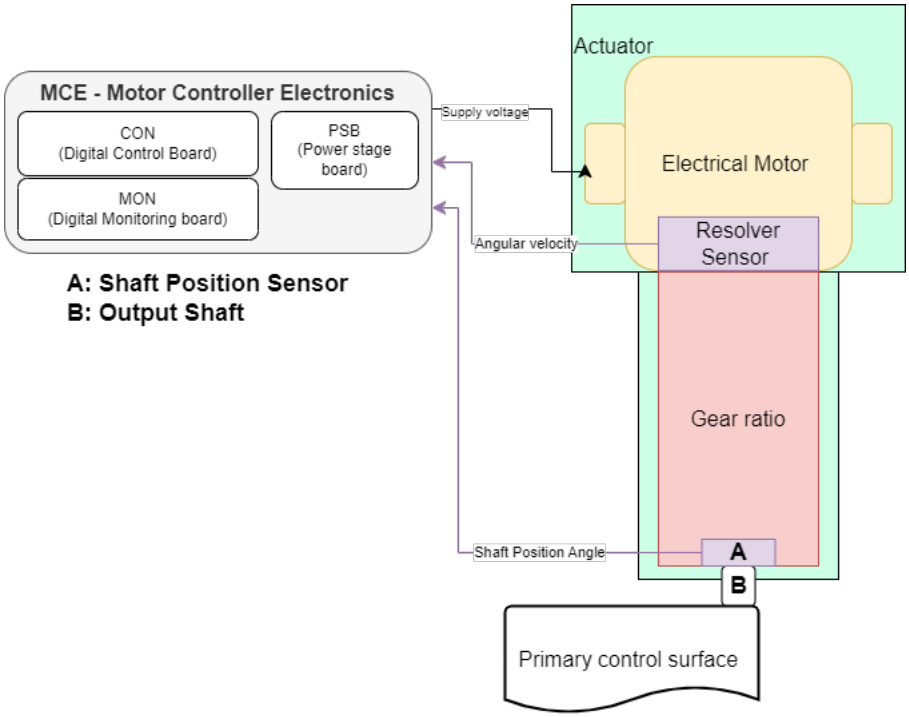

Figure 3.1: Single channel configuration

Figure 3.1 represents the single actuator configuration consisting of a single MCE, electrical motor and single set of sensors.

Tests for the Actuator

	Single Motor Actuator MCE suffers power loss with:	
Aim	Motor windings OPEN	Motor windings SHORTED
Backdrive the actuator:	Zero BEMF damping	BEMF providing induced damping
Observe damping characteristics:	Zero BEMF damping	BEMF providing induced damping
Vary gear ratio:	Vary of friction losses	Combination of friction and induced damping

Table 3.1: Functions, and cases for the single channel configuration, pure resistance is the mechanical resistance from gearing, friction and inertia.

In table 3.1 the test cases and the required model functions to study are presented. Note that friction is part of all tests, but it is expected to see a change for different gear ratio. More details regarding the cases and functions below.

Test cases:

1. The MCE suffers power loss with the motor windings open.
2. The MCE suffers power loss with short circuited motor windings.

Functions:

1. Backdriving the actuator which will result in back EMF of the motor to induce damping.

   Assumption:
   When the MCE loses power and the motor windings are shorted, an induced current appears. However some induced current should appear even with the MCE still connected but small.

2. Observe the damping characteristics for the tests as a function of the amplitude, frequency and torque resulting from different airload on the surface.

   Assumption:
   There will be an inherent force from the high gear ratio, and damping from the BEMF of the motor, depending on the impedance seen by the windings.

3. Vary the gear ratio, to observe the physical resistance of the actuator to the external force applied through the surface with the two motor winding cases.

	Single motor actuator	
	MCE suffers power loss with:	
	Motor windings OPEN	Motor windings SHORTED
Potentially desirable Yes/No	No	Yes
MATLAB Yes/No	Yes	Yes
Outcome/Consequence	No damping	Damping

Table 3.2: Single motor actuator test observations

3.2 Damping circuit design evaluation

The electric motor will create BEMF at all time. Although without providing the current any path to flow it is restricted. The short circuit, or damping circuit when a resistor is applied, enables a path for the induced current to flow and from that creating an opposing torque, BEMF. This is done with Delta-Y, Delta-Open or Delta-Delta.

CASE: Delta-Y Configuration	f[Hz]	Applied Displacement[Deg]	Angular Velocity Rotor[rad/s]	Applied Torque[Nm]	General Information
1	1	± 1	34.9261	950.9273	R_d = 100 Ω
2	1	± 10	349.2605	4.2563e+03	
3	10	± 1	347.9009	210	
4	10	± 10	3.4790e+03	2600	
5	40	± 1	1.3141e+03	3851	
6	40	± 10	1.3141e+04	3.81023+04	

Table 3.3: Results from Delta-Y damping circuit

CASE: Delta-Open Configuration	f[Hz]	Applied Displacement[Deg]	Angular Velocity Rotor[rad/s]	Applied Torque [Nm]	General Information
1	1	± 1	34.9261	349.9261	R_d=100 Ω
2	1	±10	1.7466e+03	2.9253e+03	
3	10	±1	1.5898e+03	219	
4	10	±10	1.5895e+04	2.6410e+03	
5	40	±1	2.7085e+03	3.8290e+03	
6	40	±10	2.7000+04	3.8290e+04	

Table 3.4: Results from Delta-Open damping circuit

CASE: Delta-Delta Configuration	f[Hz]	Applied Displacement[Deg]	Angular Velocity Rotor[rad/s]	Applied Torque [Nm]	General Information
1	1	±1	34.9261	353.8537	R_d=100 Ω
2	1	±10	1.7466e+03	2.9108e+03	
3	10	±1	1.5898e+03	223	
4	10	±10	1.5895e+04	2.6410e+03	
5	40	±1	2.7085e+03	3.7290e+03	
6	40	±10	2.7000+04	3.8290e+04	

Table 3.5: Results from Delta-Delta damping circuit

The different damping circuit designs generate different levels of current while being exposed to the same external force which inherently contribute to the applied torque. This can be seen in Table 3.3, 3.4 and 3.5. Although, the difference in Applied torque did not affect the generated torque greatly apart from case 1 and 2. Therefore, the decision to choose a delta-open damping circuit is based on a suggestion from Heart Aerospace to enable integration of the damping circuit within the H-bridges of the MCE to reduce the need of additional components. This is possible since both the positive and negative node of each phase goes to the same H-bridge. In figure 3.2 below the visualisation of the delta-open circuit is displayed as how it is implemented. L_{sf} and R_{sf} respectively is the representation of inductance and resistance of the coil. e represent the induced voltage and R_d is the damping circuit resistance.

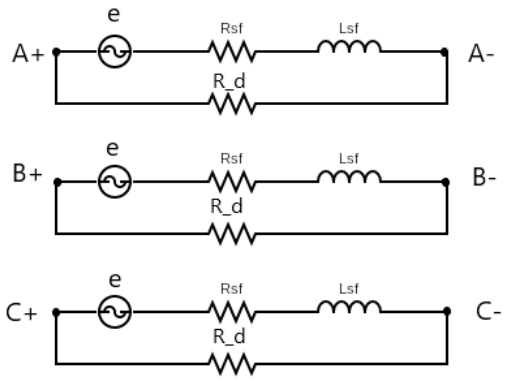

Figure 3.2: Drawing of the delta with open terminals damping circuit

3.3 System targets

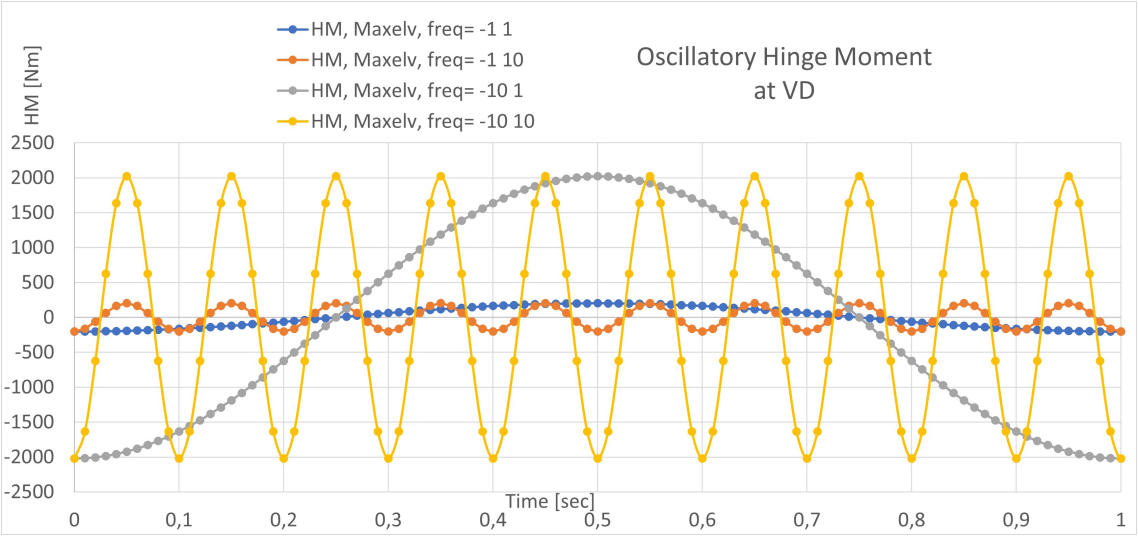

Figure 3.3: Oscillatory hinge moment at VD

In figure 3.3 four different test cases are performed with different frequencies of oscillatory hinge moments are applied. These loads are applied during Design Diving Speed, V_D which is the highest planned speed the aircraft has to achieve during testing [15]. What can be seen is that when an angular displacement of 10 degrees at 1 Hz is applied, the surface suffers from a large hinge moment during a longer time period, compared to 10 Hz that generates the high load more frequently but for a shorter amount of time. Note that these values provided by the Flight Science department at Heart Aerospace is not final nor valid for the ES-30 aircraft, but approximated values for an aircraft of the same size. The specific ES-30 aircraft aim to have a deflection range of ± 20 degrees for the elevator. To evaluate if the actuator system is sufficient for damping an external force when suffering from power loss, it is required to achieve the following:

1. **Gustlock:** That the actuator for the ES30 elevator is adequate for gust lock of 599 (Nm) wind when the aircraft is powered down.
2. **Hinge moment:** The EMA is required able to withstand 2000 Nm at the hinge line.
3. **Damping coefficient:** Provide damping coefficient of the actuator in the unit of $\frac{Nms}{rad}$.

3.4 MATLAB model

To be able to test and evaluate the actuator a MATLAB and Simulink model is developed. The Simulink model consists of an MCE block, a permanent magnetized electric motor block, a mechanical model block providing the gearing ratio and finally an external force or motion. The model includes No Load Running Torque

(NLRT), torque needed to spin the thrust bearings, also without axial load on it. It does not include breakout friction, that is when an object is to start a motion it requires more force than to keep it in motion. To conclude, breakout friction is the friction from stationary to a movement while NLRT is to keep the movement constant even without load. The breakout friction can be disregarded as it will only affect for low forces, and this thesis test worst case scenarios.

3.4.1 Mechanical model

Figure 3.4 below includes four main components.

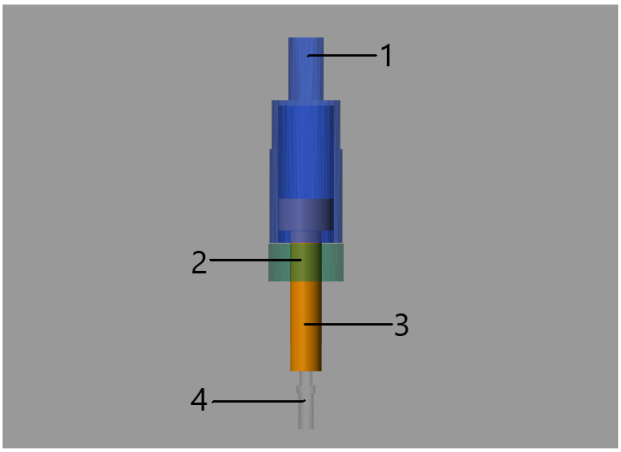

Figure 3.4: MATLAB/Simulink actuator representation

1. The output shaft
2. Fixed ballnut
3. Shaft
4. EM rotor

Note that this is a simplification from the real model. The ball-nuts internals is not modelled, but this is reasonable since the friction from it is implemented.

3.4.2 Electric motor

The electric motor used in this thesis is a Brush-Less Permanent Magnetised Synchronous Motor, or Brushless AC-Motor, BLAC. The following parameters is used thorughout this thesis:

- $R_{sf} = 3.4\ \Omega$
- $L_{sf} = 0.0139$ H
- $K_t = 2.1390\ \frac{Nm}{A_{max}}$
- $K_{ef} = 1.1140\ \frac{V_{ph,max}s}{rad}$
- PP = 10

Where R_{sf} represent the resistance in each coil and L_{sf} the inductance of each coil. K_t and K_{ef} is the torque constant and motor constant of the electric motor, pp is the number of pole-pairs.

Calculating the induced voltage and torque for one phase

$$\theta = \mod(\theta_e, 2\pi) \qquad [rad] \tag{3.1}$$
$$e = -K_{ef} w_r \qquad [V] \tag{3.2}$$

Where θ_e is the mechanical position of the rotor in radians multiplied by the pole pair.

$$\theta_e = \theta_m pp \tag{3.3}$$

From the induced voltage together with the coil impedance Z_{sf}, from R_{sf} and L_{sf} the induced current is created.

$$i = \frac{e}{Z_{sf}} \qquad [A] \tag{3.4}$$

When the induced current is defined the torque, BEMF, is derived. Negative sign since the BEMF is of opposite direction to the angular velocity.

$$\tau_{onephase} = -\frac{2K_t}{3} \cdot i \qquad [Nm] \tag{3.5}$$

In a three phase electrical motor this requires a few extra steps. The electrical fields is separated by 120 degrees. The first step is therefore to define the angle of the different phases as in equation 3.1

$$\theta_{A,B,C} = [\ \mod(\theta_e, 2\pi), \quad \mod(\theta_e - \frac{2\pi}{3}, 2\pi), \quad \mod(\theta_e - 2\frac{2\pi}{3}, 2\pi)] \tag{3.6}$$
$$e_{normalized} = interpolation(bemf_v, theta_v, \theta_{A,B,C}) \tag{3.7}$$
$$e_{A,B,C} = -K_{ef} \cdot \omega_r \cdot e_{normalized} \qquad [V] \tag{3.8}$$

Therefore when calculating the induced voltage e the interpolation provides input on how much voltage and torque can be extracted from each phase. Depending on the position of the induced magnetic field relative to the magnets, so it provides a normalized value between ± 1. The values of $bemf_v$ and $theta_v$ can be found in appendix. Lastly this was done by the interpolation in equation 3.7 represented in figure 3.5.

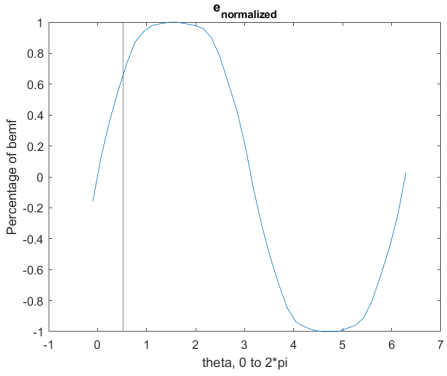

Figure 3.5: The interpolation providing $e_{normalized}$

The vertical line represents the angle of $\theta_{A,B,C}$ for each phase and at the point where the line cross the trapezoidal curve is the normalized value of how much torque is generated in each phase. Then by extending equation 3.5 with $e_{normalized}$ the total induced torque from BEMF result in equation 3.9.

$$\tau = \frac{-2}{3} K_t (e_{normalized,A} i_A + e_{normalized,B} i_B + e_{normalized,C} i_C) \quad \left[Nm \right] \tag{3.9}$$

3.4.3 Motor control electronics

The MCE consists of power supply, H-bridges, an RC-circuit, controllers and a brake circuitas mentioned in section. The power source to the MCE will be set to an open circuit to emulate power loss.

RC-circuit

This circuits purpose is to keep the voltage provided to the H-bridges constant and smoother if there is any noise in the power supply.

H-bridges

The independent H-bridges consists of four MOSFETS and provide a smooth sinusoidal signal to each phase of the electric motor. The H-bridges itself is controlled by the PWM signals provided from the controllers.

4

Results

As mentioned in section, to determine if electromechanical actuators is suitable for the primary control surfaces on an aircraft it is desired to act similarly to a hydraulic actuator. For the power supply failure case this means emulating a similar damping characteristic. Applied torque, T, is the amount of torque required to rotate the output shaft at the desired angular velocity, to overcome the combined forces of gear ratio, friction and induced torque from BEMF. Applied motion refers to the desired angular velocity as input to the system.

In Section 4.1 the impedance of the MCE is evaluated to ensure it provides enough impedance for the actuator to not act as a generator without the damping circuit, or short circuit. Section 4.2 addresses the external forces impact to the system, that is to understand the systems behaviour purely as a function of frequency. Furthermore 4.3, 4.4 analyze the actuators internal friction and BEMF respectively and how it affects the applied torque. Finally section 4.5, 4.6 and 4.7 tests the system targets mentioned in section 3.3.

4.1 Impedance of Motor Control Electronics

When the MCE suffers from power loss the EM still creates a BEMF, and the induced current inherently try to flow through the phases H-bridges to the MCE's RC-circuit. Figure 4.1 concludes that the impedance of the MCE itself in a power loss situation is very high. Since it is not possible to change the RC-circuit without affecting the active case, the impedance remains unchanged. A conclusion from this is to disconnect the MCE and create a damping circuit separated from the MCE to generate a high BEMF.

4.2 External forces frequency impact

In figure 4.2 a frequency load is applied on the output shaft in order to see the behavior of the position. With increased frequency the change in positions decreases, which is seen in the decrease of amplitude in the blue (top) graph. Meanwhile the frequency of the angular velocity increases (bottom, red), but the amplitude remains fairly unaffected.

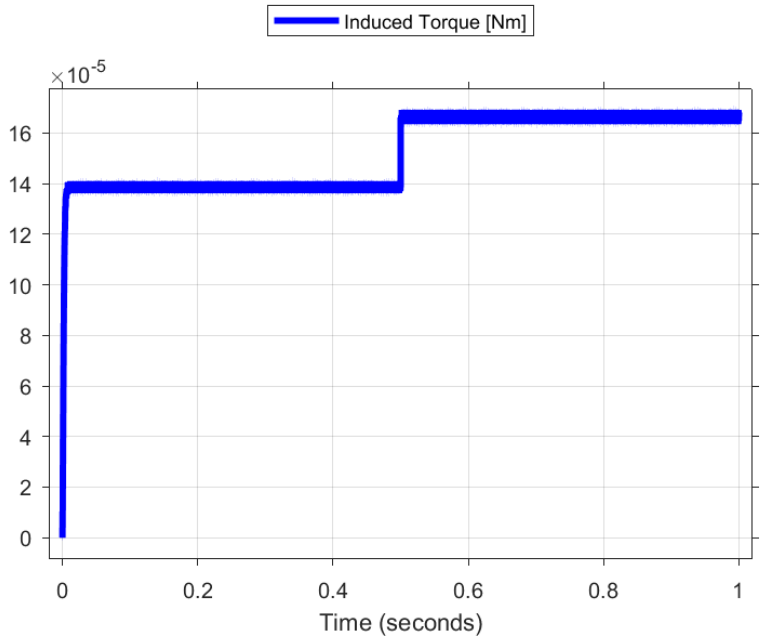

Figure 4.1: Induced torque, time instance 0-0.5s disconnected from MCE, 0.5-1s connected to the MCE

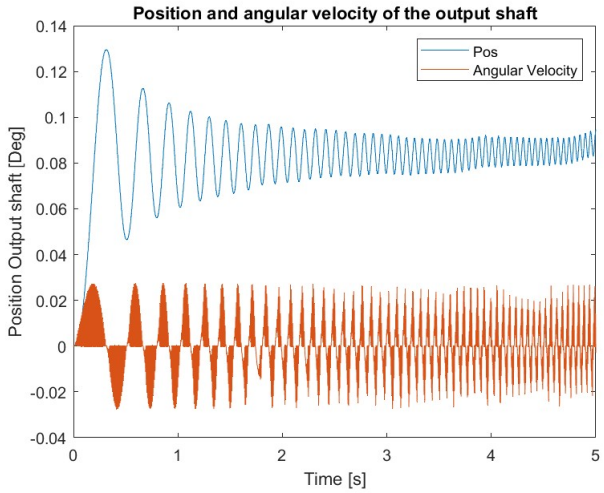

Figure 4.2: Position (deg) and angular velocity (deg/s) of the output shaft during increased frequency of the applied torque on the output shaft.

4.3 Actuator friction

The mechanics of the EMA contain two types of friction, viscous friction from the lubricant and dry friction that appears from surfaces sliding across each other in pre-loaded bearings. The simulations are done with and without the friction to see the contribution. The contribution from the friction depends on two factors, velocity and torque, creating a non-linear behaviour in the actuator. In figure 4.3 a ramp

of 5 degrees per second is applied with and without friction, both cases have the damping circuit connected.

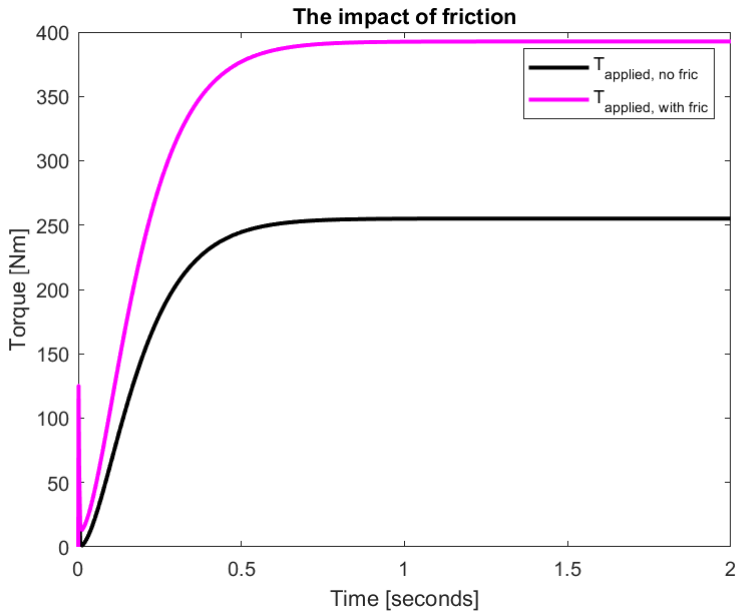

Figure 4.3: Applied torque with and without friction. Input was applied motion of 5 $\frac{deg}{s}$.

In another test an applied motion or torque on the output shaft caused the rotor to accelerate until the external impact was removed. In the model without any friction it continues to rotate at constant angular velocity, while in the model with friction applied it slow down to a stationary point. This validated the frictions contribution in the model.

4.4 Characteristics of back electromotive force

Since the induced voltage depends on the angular velocity of the rotor and motor constant K_{ef}, in equation 4.1, and thereby the angular velocity on the output shaft, a motion is applied there. By applying a ramp with constant gradient and measure the applied torque the characteristics of the system are determined.

$$BEMF = K_{ef} \cdot \omega_r \tag{4.1}$$

deg/s	Applied Torque[Nm]
0.1	12.5234
1	82.3926
2.5	198.7825
5	392.3742
10	776.5668
15	1.1541e+03
20	1.5219e+03

Table 4.1: Applied torque on the output shaft

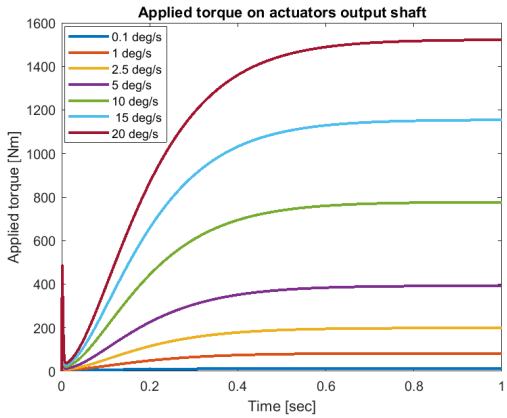

Figure 4.4: Torque curve from different applied ramps

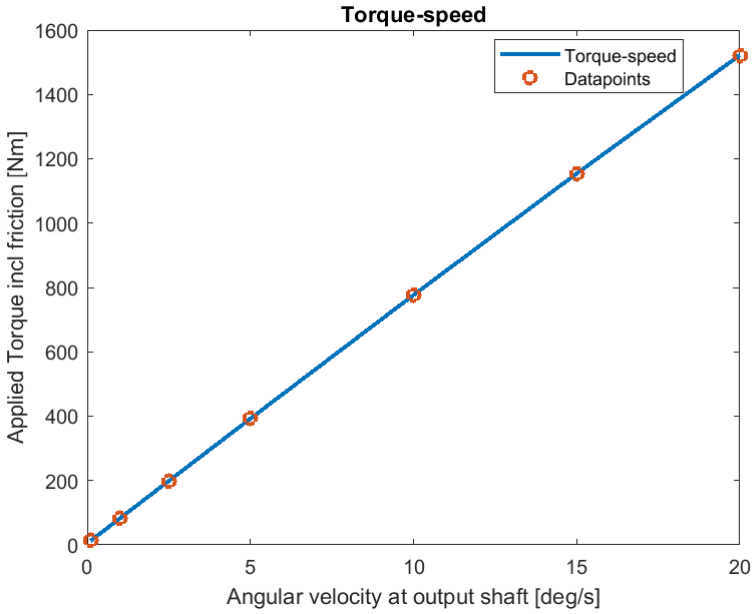

Figure 4.5: The motor is connected to the damping circuit from the initial time step with $R_d = 100\Omega$ and various ramps applied to the output shaft.

To achieve the results in table 4.1 and figure 4.4 the standard a motion as input. Table 4.1 consists of the final values from the graphs presented in figure 4.4. Using these values a torque-speed characteristics curve could be produced in figure 4.5. This implies that it is possible to approximate a linear torque-speed characteristics at low angular velocities. In figure 4.6, a sinusoidal motion is applied to the output shaft that varies between ± 10 deg at 5 Hz. The combination of the angular displacement

and the frequency creates higher angular velocities than in figure 4.5 providing a different characteristic.

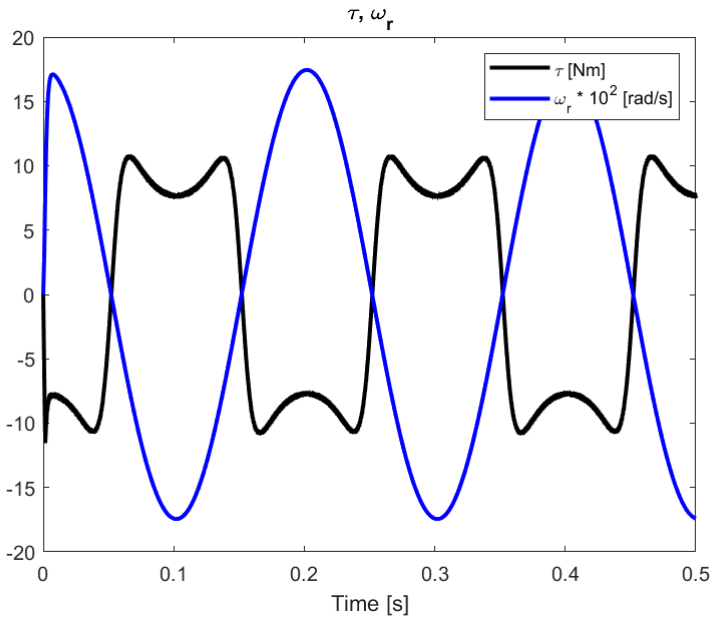

Figure 4.6: Induced torque τ from BEMF and angular velocity of the rotor ω_r rad/s

By studying a cycle of the angular velocity, ω_r, and the induced torque, BEMF in figure 4.6, the actuators total torque-speed curve are produced in figure 4.7

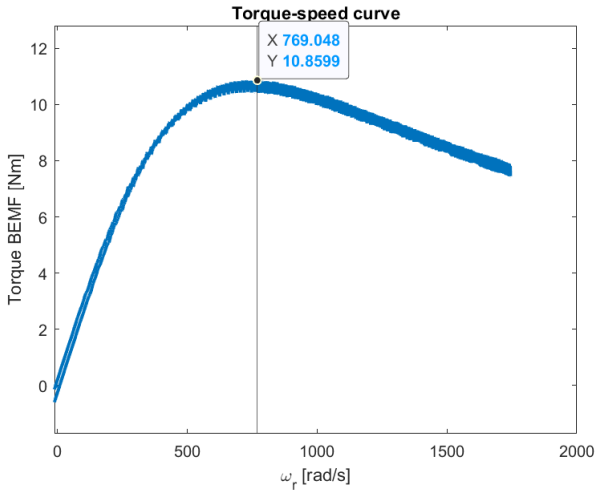

Figure 4.7: Torque-speed curve of the electric motor

Conclusions from figure 4.7 is that induced torque from the electric motor decrease after a certain angular velocity of the rotor, i.e. the torque-speed curve is not linear. Thus, the peak-value of the torque speed curve is desired to not exceed to keep sufficient damping, this behaviour is reasonable because of equation 4.2.

$$P = \tau \cdot \omega_r \quad \left[W\right] \tag{4.2}$$

This is what is causing the hammock shape of the induced torque. The intersection between the vertical line and the torque-speed curve in figure 4.7 represent the angular velocity that provide the highest amount of torque for $R_d = 100\Omega$.

$$\omega_{r,max} = 762.628\frac{180}{\pi} \approx 43695 \quad \left[\frac{deg}{s}\right] \tag{4.3}$$

$$\omega_{os} = \frac{w_{r,max}}{gearRatio} \approx 137.19 \quad \left[\frac{deg}{s}\right] \tag{4.4}$$

By dividing by the gear-ratio the angular velocity of the output shaft is derived and a unit change from radians to degrees provide that 137.19 $\frac{deg}{s}$ is the angular rate that produce the highest damping torque for this specific electric motor. Therefore, since it is desired to have a higher amount of torque with the same gear ratio, another electric motor is required. This is visually displayed in figure 4.8 as the power's rate decrease as ω_r increase. Note that the scaling of ω_r and power P is different to fit in the same figure as the induced torque.

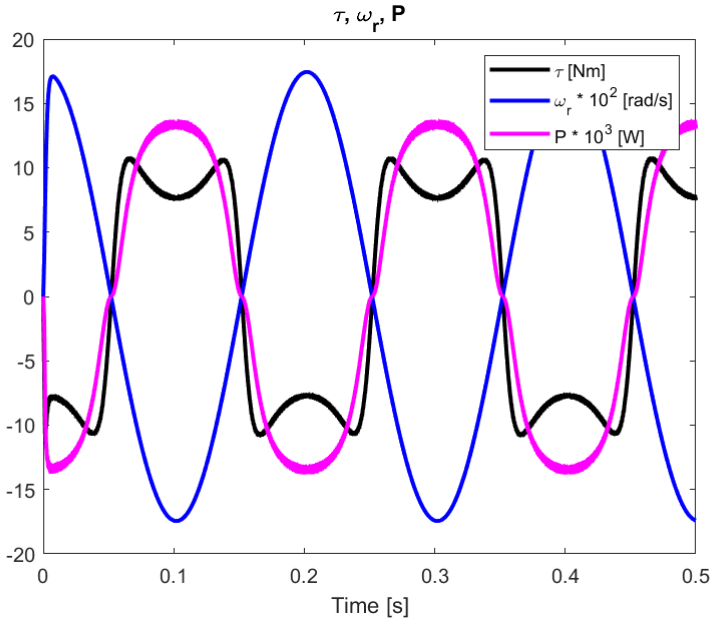

Figure 4.8: Induced torque τ (Nm) together with rotor angular velocity ω_r (10^2 rad/s) and the Power P (W)

In figure 4.9 the applied torque is presented with increasing applied motion as input, to determine the full actuators torque-speed curve. This results in a maximum torque, $T_{Max} \approx 5270$ Nm, appearing again at $\omega_{os} \approx 137$ $\frac{deg}{s}$ with friction.

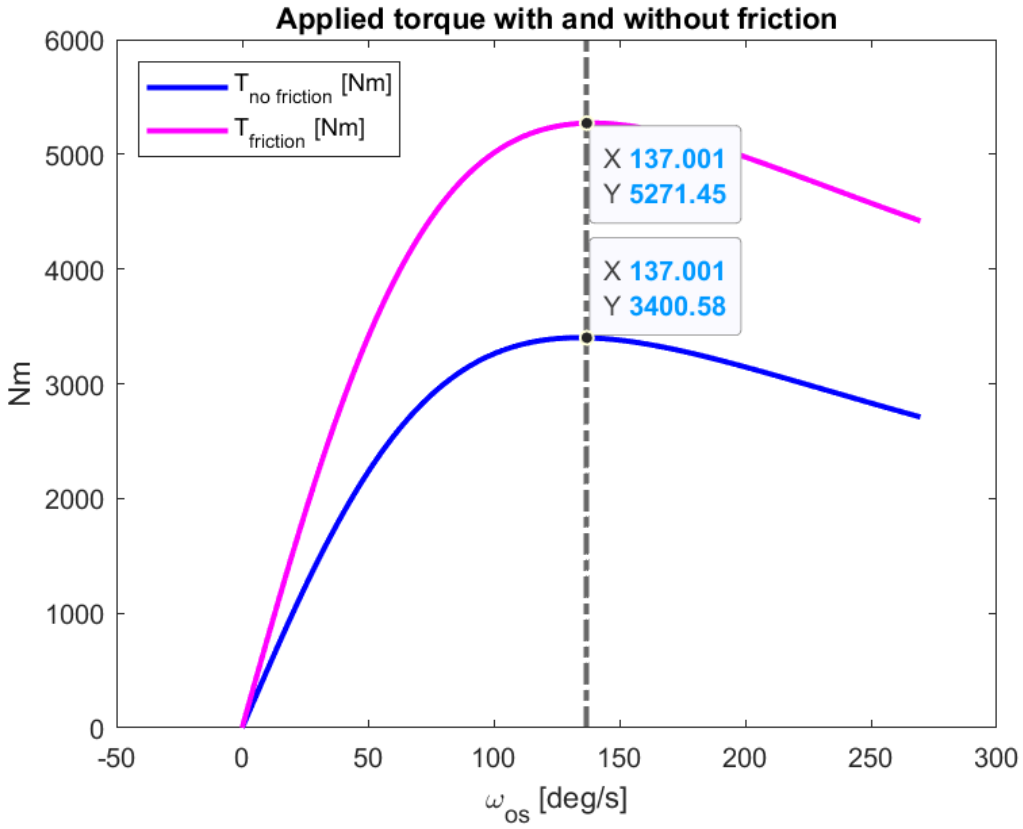

Figure 4.9: Maximum applied torque with and without friction by an increasing ramp as applied motion in $\frac{deg}{s}$, torque in Nm

4.5 Damping

The damping characteristics of the system are analyzed based on the damping coefficient in $\frac{Nms}{rad}$. Additionally a relation between the damping coefficient and the damping circuit resistance is found.

$$c = \frac{\tau}{\omega_r} = \frac{Nm}{rad/s} \tag{4.5}$$

$$e = i(R_d + R_{sf}) + L_{sf}\frac{di}{dt} = K_{ef}\omega_r \tag{4.6}$$

$$\tau = \frac{-2}{3}K_t i \tag{4.7}$$

The induced torque has a negative sign because the generated torque oppose the rotation. Rewriting equation 4.7 provides:

$$i = \frac{-3\tau}{2K_t} \tag{4.8}$$

By combining equation 4.6 and 4.8 equation 4.9 is provided:

$$\frac{-3\tau}{2K_t}(R_d + R_{sf}) + L_{sf}\frac{di}{dt} = K_{ef}\omega_r \tag{4.9}$$

For low angular velocities the frequency of the induced currents is low. Therefore, the effects from the inductance is low and can therefore be neglected in the linear stages of the torque-speed graph. Note that in equation 4.10 it is easy to change between R_d value and c depending on which is known. For instance determine damping coefficient for a certain R_d or determine R_d to achieve a fixed damping coefficient.

$$\frac{\tau}{\omega_r} = \frac{-2K_{ef}K_t}{3(R_d + R_{sf})} = c \tag{4.10}$$

Figure 4.10 is created using equation 4.5 with τ from phase A, induced torque from

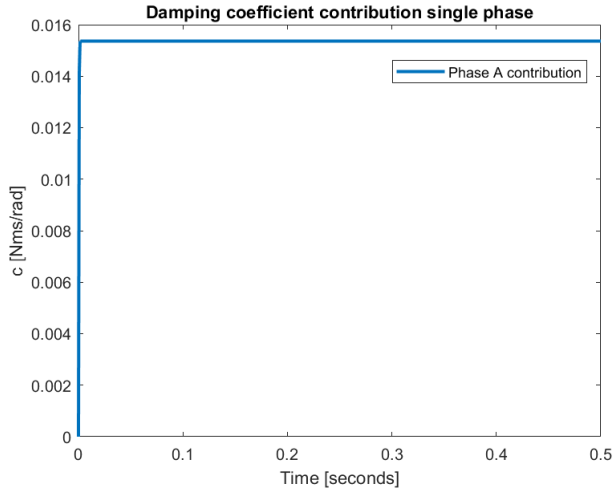

Figure 4.10: Damping contribution from phase A

the phase A, and a constant angular velocity of 20 degrees per second on the output shaft. Using equation 4.10 and the parameters the damping coefficient contribution is verified.

- $K_{ef} = 1.1140 \ \frac{V_{ph,max}s}{rad}$
- $K_t = 2.1390 \ \frac{Nm}{A_{max}}$
- $R_d = 100 \ \Omega$
- $R_{sf} = 3.4 \ \Omega$

$$c_{analytical} = \frac{2 \cdot 1.1140 \cdot 2.1390}{3(100 + 3.3995)} \approx 0.0154 \tag{4.11}$$

Therefore, changing the size of the resistor in the damping circuit determines the amount of induced torque that are produced at what angular velocity, ω_{os}.

In figure 4.11, the damping coefficient contribution from phase A, B, C, and the final damping coefficient at a constant applied velocity with $R_d = 100\Omega$ in the damping circuit.

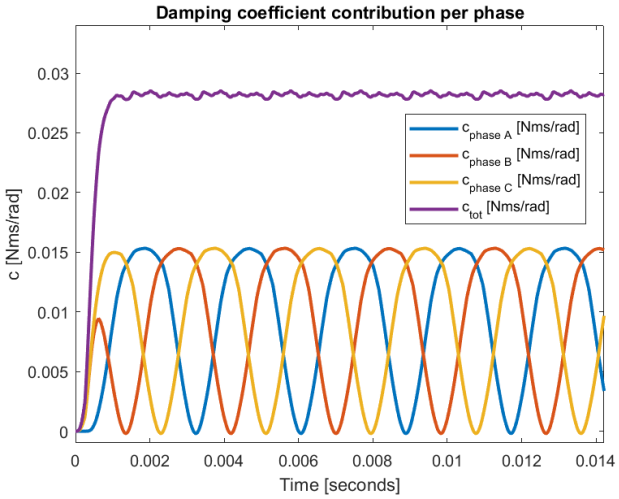

Figure 4.11: Damping coefficient contribution from each phase, the sum of them and the final damping coefficient for an angular velocity at the rotor corresponding to $\omega_{os} = 20$ deg/s at the output shaft

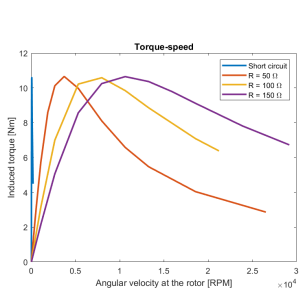

(a) Torque-speed graph

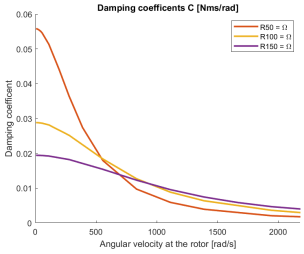

(b) Damping coefficient graphs

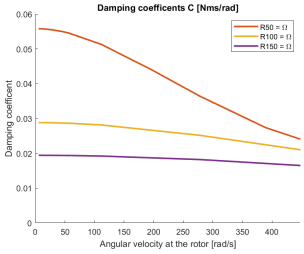

(c) Damping coefficient graphs zoomed in

Figure 4.12: Effects of changing the size of the resistor

The change of resistance in the damping circuit has a crucial effect on the characteristics of the BEMF from the electric motor and therefore the induced torque. In figure 4.12, both the torque-speed and the damping coefficient vary greatly depending on the size of the resistor. The dead-short is not included in the damping coefficient graph because it provided a high initial value followed by dropping to zero immediately. Increasing the resistor extend the torque-speed curve but never change the peak value. Looking at the damping coefficients in figure 4.12c a trade-off is visible. Lower resistance provide a higher damping coefficient but at the cost of a smaller damping range, while a higher resistance provides a smaller damping coefficient but for a wider range of ω_r.
According to Turunen et al. [16], the damping estimation of a system can be studied by applying an impulse signal to the electric motor and then fit a curve to the position of the rotor. By applying an impulse to the output shaft, top left of figure 4.13, for a short instance it is possible to see the damping occur. Bottom left is the position of the output shaft in degrees, top right is the position of the rotor in radians and finally the bottom right is the angular velocity of the rotor. Since

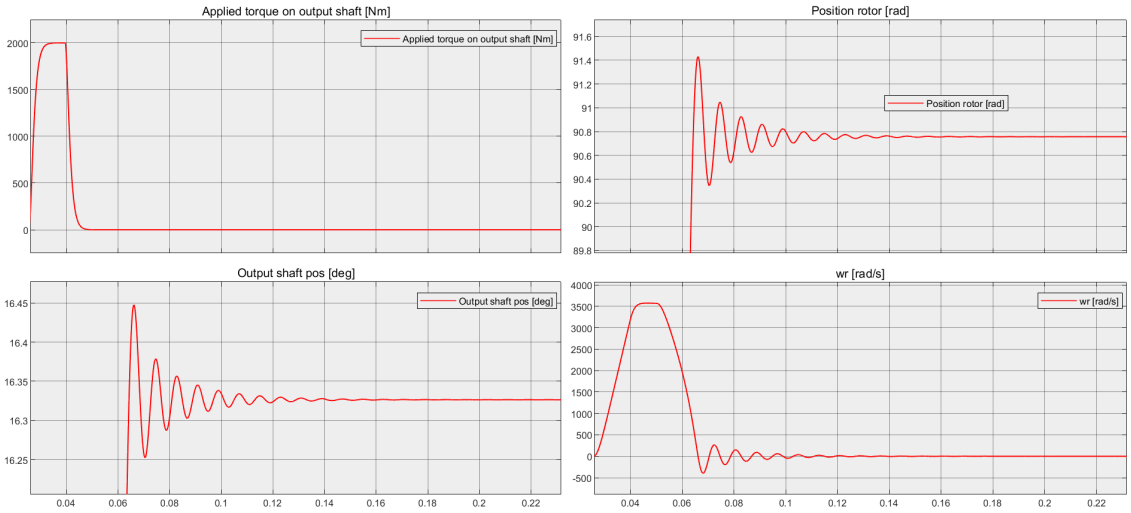

Figure 4.13: Proof of damping with $R_d = 100\Omega$, connected to the damping circuited at t = 0.05 s

the rotor and output shaft are mechanically attached, the factor of the gear ratio separates them. By collecting each coordinate of the peaks for the output shafts damping and center around 0 bias the relation in figure 4.14 is constructed.

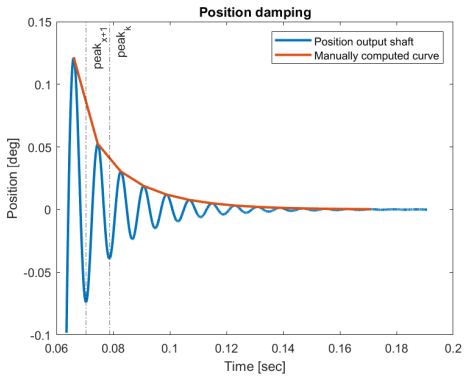

(a) Position damping with manually fitted damping curve

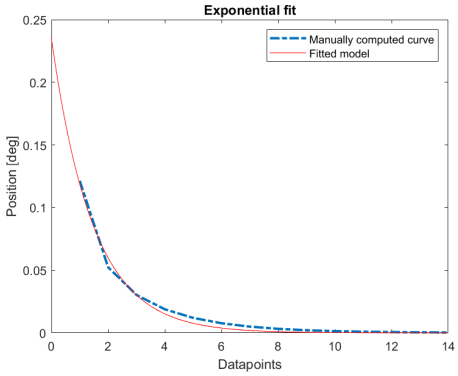

(b) Exponential fitting to the manually fitted damping curve (Original data points)

Figure 4.14: Damping of the output shafts position from an applied torque impulse

Furthermore the natural frequency w_n is derived.

$$\omega_n = \frac{w_t}{\sqrt{1-\xi^2}} \tag{4.12}$$

$$\omega_t = \frac{2\pi}{\Delta t} \tag{4.13}$$

The natural frequency, ω_n, is dependent on the damping ratio ξ and the frequency of the attenuating oscillation, ω_t. Δt is the period time for one oscillation and thereby the time difference between two peak values, as the difference between $peak_k$ and

$peak_{k+1}$ in figure 4.14a . Rearranging the equations:

$$\omega_n = \omega_t - \xi\omega_n \tag{4.14}$$

To determine the damping ratio via an impulse signal according to Turunen the exponential function 4.15 can be applied.

$$y = ae^{-\xi\omega_n t} \tag{4.15}$$

$$y = Ae^{Bt} \tag{4.16}$$

By using the MATLAB function *fit*, an approximated curve can be created with an exponential expression, equation 4.16 and compare to equation 4.15. Identification between the equations gives the relations seen in equation 4.17:

$$B = -\xi\omega_n \quad and \quad A = a \tag{4.17}$$

Through the relation seen in equation 4.17, since w_t and B are known, w_n is found and presented in equation 4.18.

$$\omega_n = \omega_t - B \tag{4.18}$$

Finally the damping ratio is presented as

$$\xi = \frac{\omega_t - \omega_n}{\omega_n} \tag{4.19}$$

4.6 Behaviour at constant applied torque

I figure 4.15a a constant torque of 2000 Nm at t = 0.02 has been applied. This generates the induced torque in figure 4.15b with the output shaft position in figure 4.15. The resistance in the damping circuit is decreased in an attempt to find the highest damping. Increasing the resistance increases the initial peak, while a decreased resistance decreases the peak. However, it stabilizes around 4 Nm for all tested resistors between 1 to 150 Ω. Furthermore, this proves that the system is able to provide continuous damping throughout the resistance interval that was tested.

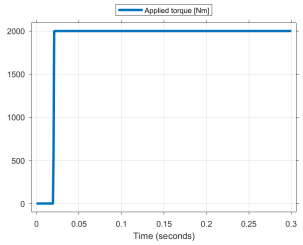

(a) Applied torque

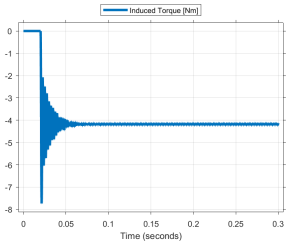

(b) Induced torque, τ

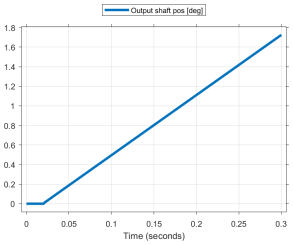

(c) Position of shaft

Figure 4.15: Applied torque, τ and position for a constant applied torque of 2000 Nm
Note: $R_d = 20\Omega$

4.7 Gust Lock

In figure 4.16 a torque of 599 Nm is applied on the output shaft and analyzed with four different resistors. In order for the EMA to act as a Gust Lock the surface is required to not slam the end position with a high impact force. With the four different resistances, 25, 50, 75 and 100 Ω the EMA is driven for 5 seconds in order to see how long it would withstand the external torque. With 100 Ω, the EMA hits the end position quickly, nearly 3 second after the start. Although, the choice of 25 Ω makes the EMA able to withstand the external force for the entire simulation time without reaching the end position.

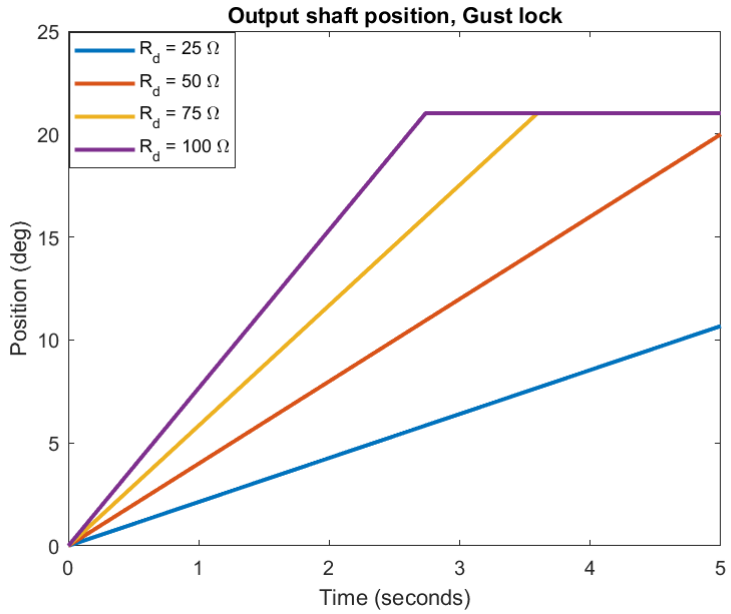

Figure 4.16: Position of the output shaft with various resistors in the damping circuit

Thus the angular velocities also vary with the size of the resistors. ω_r is proportional to the gust lock position figure 4.16, as the reached position reflects the angular velocity. Comparing figure 4.17 and 4.18, the damping circuit with $R_d = 25\Omega$ provide the lowest ω_r, hence the lowest impact to the end position.

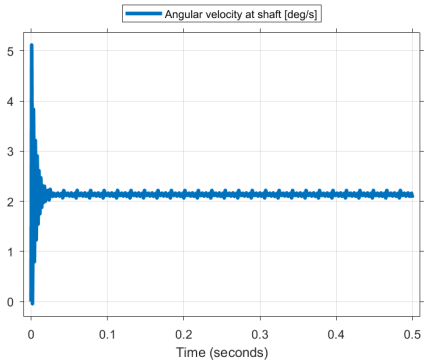

(a) Angular velocity $R_d = 25\Omega$

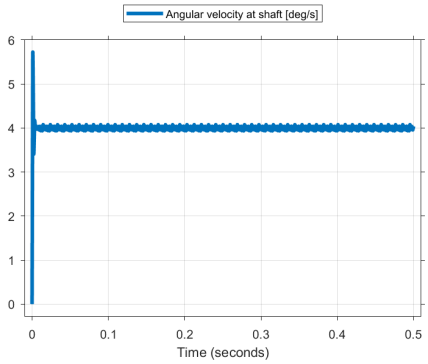

(b) Angular velocity $R_d = 50\Omega$

Figure 4.17: Angular velocity at output shaft with $R_d = 25\Omega$ vs $R_d = 50\Omega$

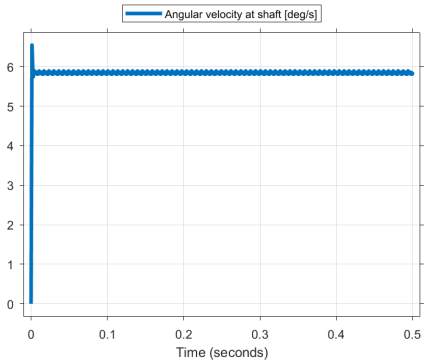

(a) Angular velocity $R_d = 75\Omega$

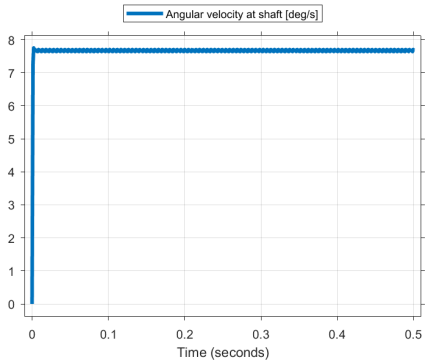

(b) Angular velocity $R_d = 100\Omega$

Figure 4.18: Angular velocity at output shaft with $R_d = 75\Omega$ vs $R_d = 100\Omega$

5

Discussion

This thesis has evaluated the possibility for an electromechanical actuator for the aviation industry to withstand external forces while suffering from power loss. A simulation environment in Simulink has been developed by the help of UMBRA-GROUP, with a model consisting of one electrical motor connected to a mechanical transmission. Also, an evaluation regarding the actuator's ability to act as a gust lock was made.

5.1 Electromechanical Actuator

The EMA for this analysis, consisted of one electric motor and was therefore not the exact actuator intended for the aircraft. One can therefore assume the dual EM configuration of the actuator will provide more opposing force to the external forces. The single EM configuration was in order to see if one motor is strong enough to provide power in a damping mode. If one motor will generate enough induced torque in order to provide damping during power loss, the dual system configuration will also be able to provide sufficient damping. The damping characteristics has been evaluated with applied torque or applied motion on the output shaft. However, this is not enough to decide whether the EMA is sufficient for flutter prevention explained in section 2.10. Since flutter is a more complex phenomenon and has not been deeply investigated in this thesis.

5.2 Motor Control Electronics

The MCE's impedance is too high to be sufficient for damping. This resulted in an external damping circuit that can, if desired, be implemented in the H-bridges of the MCE. The alternative to change further components inside the MCE is not advantageous due to the effect of the active case which the MCE must be designed for. The high impedance of the MCE is suitable for the dual motor configuration. If one of the motors suffers power loss, it should not act as a generator and thereby fighting the active motor. The high impedance create a very low induced torque and therefore, since the MCE have high impedance, it will generate voltage but almost no current.

5.3 Friction

The result of the actuators friction is positive for the damping. The friction provides a lot of force that is opposed to the motion at higher angular velocities. This combination with the BEMF is beneficial in order to damp the control surface. As with an hydraulic actuator, pushing the surface slowly is possible even with this EMA. Pushing the surface quickly and hard will enable a fast movement until almost becoming stationary as the oil is compressed, this is also expected from the EMA as the contribution from the frictions is increased with speed. This can be seen in figure 4.9.

5.4 Back electromotive force

The BEMF from the EM seems to be high enough to withstand the forces required. The highest induced torque generated by BEMF from the motor is 10 Nm, which by the gear ratio equals 3185 Nm on the output shaft when disregarding eventual losses. However the maximum force is momentarily and sizing of the damping circuit resistance need to be evaluated for ideal bandwidth of the system. The EM provides a linear induced torque for the low ω_r. It is advantageous to stay within the linear area of the torque-speed curve to not overheat the motor. That is because increasing ω further will induce higher currents that can damage the electric motor over time. If the angular velocity providing the maximum torque appears, it will most likely decrease in speed close to instantly which will decrease the induced current and thereby not overheat the motor.

5.5 Damping ability

The induced current from the EM with the damping circuit generates an induced torque that together with the gear ratio is strong enough to pass the requirements for withstanding an external force with a significant margin. With an increasing frequency of the external force, the position of the angular displacement decreases. By the help of the Flight Science team at Heart Aerospace, a characteristic equivalent of what flutter could look like was developed. The bandwidth of the motor will depend on the resistance in the damping circuit, with a trade-off between high torque at low, medium or high angular velocities. The impulse signal of the applied torque gives an intuition of the systems damping ability. It handles a disturbance well by going to a stationary position after a short transient phase.
Since the actuator requires a motion to be able to withstand forces with the current design choices, once the surface are stationary it looses the induced torque. However, with a constant external force in section 4.6 the damping is evaluated with four different resistors. All four results proves that a constant damping force is enabled if the external force keeps pushing the primary control surface, but with various torque.

5.6 Gust lock

The EMA can act as a Gust lock depending on the chosen resistance in the damping circuit. Because of a big difference in frequency and torque between flutter prevention and gust lock, it is not likely that they require the same resistance. Since the angular velocity for gust lock is lower than for flutter prevention the ideal resistor is probably lower to prevent high impact to the end positions.

6
Conclusion and future work

In conclusion, using an electromechanic actuator for flutter prevention during power loss looks positive. The amount of force to rotate the output shaft, applied torque, is greater than the required 2000 Nm. Furthermore, the system is suitable for different angular velocities by sizing the resistor in the damping circuit. The system is therefore adaptable for several purposes.
To be able to determine a suitable damping ratio the maximum torque and frequency it should work with need to be decided. Furthermore, the MATLAB/Simulink model could be improved by including break-out friction. When an oscillatory load is applied, and the motor is connected to the damping circuit, this force the output shaft nearly stationary. However since the BEMF is proportional to the angular velocity it will be close to zero at stationary time instances, enabling the surface to restart the movement. A breakout friction should be implemented to enable a more realistic start of the movement as this can affect for smaller external forces. This study have not included any component failures. To be able to conclude the actuators suitability in the aviation industry several component failures need to be studied and evaluated. The dual EM configuration need to be studied, to ensure that a failed motor will not act as a generator and force-fight the working motor. The presented result that the MCE itself creates a very high impedance is positive for this purpose as it prevent the EM to act as a generator.

Bibliography

[1] title=Primary Flight Control Hydraulic Actuation System Interface Definition, author=A-6A3 Flight Control and Vehicle Management Systems Cmt, month=oct, year=2015, doi=https://doi.org/10.4271/AIR4922A, url=https://doi.org/10.4271/AIR4922A,

[2] title=Development of a reliable electro-mechanical actuator for primary control surfaces in small aircrafts, author=Mazzoleni, M. and Maccarana, Y. and Previdi, F. and Pispola, G. and Nardi, M. and Perni, F. and Toro, S., booktitle=2017 IEEE International Conference on Advanced Intelligent Mechatronics (AIM), year=2017, volume=, number=, pages=1142-1147, doi=10.1109/AIM.2017.8014172

[3] title=Hydraulic Actuators, author=Lukasz Stawinski, note=https://encyclopedia.pub/entry/8168, note=Acessed 17-05-23

[4] title=Research and modeling of force fighting equalisation for aircraft rudder's triple active actuation system, volume=126, DOI=10.1017/aer.2022.21, number=1304, journal=The Aeronautical Journal, publisher=Cambridge University Press, author=Li, D.W. and Lin, M.X. and Tian, L., year=2022, pages=1801–1814

[5] title=What is a Permanent Magnet Synchronous Motor & Its Working, author=Administration of Elelctronics|Projects|Focus, note=`https://www.elprocus.com/what-is-a-permanent-magnet-synchronous-motor-its-working/`, note=Accessed 24-05-23

[6] title=Horizontal Stabilizer-Elevator, author=Tom Benson, note=https://www.grc.nasa.gov/www/k-12/VirtualAero/BottleRocket/airplane/elv.html, note=Accessed 17-05-23

[7] title=Mosfet 1, author=Ralph Locher, Application Note 558, Rev B, October 1998, Introduction to Power MOSFETs and their Applications `http://mac.mf3x3.com/ELECTRIC_2/Fairchild/FC%20MOSFETS.pdf`

[8] article, title = H Bridge DC Motor Driver Design and Implementation with Using dsPIC30f4011, author = Özer, Tolga and Kivrak, Sinan and Oğuz, Yüksel, year = 2017, month = 05, pages = 75-83, volume = 6, journal = International Journal of Innovative Research in Science, Engineering and Techno

[9] fundament, title = RC Circuits, author = libretext, note = `https://batch.libretexts.org/print/url=https://phys.libretexts.org/Bookshelves/University_Physics/Book%3A_University_Physics_(OpenStax)/Book%3A_University_Physics_II_-_Thermodynamics_`

Electricity_and_Magnetism_(OpenStax)/10%3A_Direct-Current_Circuits/10.06%3A_RC_Circuits.pdf, note = Accessed: 16-5-2023,

[10] title=Three-Phase Connections, author=LibreTexts, note=https://batch.libretexts.org/print/url=https://eng.libretexts.org/Bookshelves/Electrical_Engineering/Electronics/Book:_AC_Electrical_Circuit_Analysis:_A_Practical_Approach_(Fiore)/09:_Polyphase_Power/9.3:_Three-Phase_Connections.pdf, note=Accessed 17-05-23

[11] @bookLiu, Tang, Sharma, Rodinov_2019, place=Gothenburg, edition=1st edition, title=Electrical Machines, ISBN=ISBN, publisher=Springer, author=Liu, Yujing; Tang, Junfei; Sharma, Nimananda; Rodinov, Artem, , year=2019, month=Oct. , page 15-17

[12] title= An observation based control approach, author=R. Delpoux, X. Lin-Shi, X. Brun, Torque ripple reductions for non-sinusoidal BEMF Motor : An observation based control approach**Financial support is acknowledged from Chassis Brakes International (CBI), Drancy, France, in the context of a collaboration between the Ampère Laboratory and Chassis Brakes International (CBI), IFAC-PapersOnLine, Volume 50, Issue 1, 2017, Pages 15766-15772, ISSN 2405-8963, https://doi.org/10.1016/j.ifacol.2017.08.2311. (https://www.sciencedirect.com/science/article/pii/S2405896317331257)

[13] Chad.H et.al. *Aerodynamic Flutter*(NextGen Aeronautics, USA, 1996)

[14] , title=Flight Control Locks , author=SKYbrary, note=https://skybrary.aero/articles/flight-control-locks, note=Accessed 16-05-23,

[15] title=Advisory Circular , author=U.S. Department ofTransportation, note=https://www.faa.gov/documentLibrary/media/Advisory_Circular/25-335-1a.pdf, note=Accessed 24-05-23,

[16] title=Comparison of Three Electromechanical Oscillation Damping Estimation Methods, author=Turunen, Jukka and Thambirajah, Jegatheeswaran and Larsson, Mats and Pal, Bikash C. and Thornhill, Nina F. and Haarla, Liisa C. and Hung, William W. and Carter, Alex M. and Rauhala, Tuomas, journal=IEEE Transactions on Power Systems,
year=2011, volume=26, number=4, pages=2398-2407, doi=10.1109/TPWRS.2011.2155684

[17] Gustaver, M. (2020) A Chalmers University of Technology Master's thesis template for LaTeX. Unpublished.

A

Appendix 1

```
tetae_v=[0.00 0.17 0.35 0.52 0.69 0.86 1.04 1.21 1.38 1.56 1.73 1.90 2.07 ...
         2.25 2.42 2.59 2.76 2.94 3.11 3.28 3.46 3.63 3.80 3.97 4.15 4.32 ...
         4.49 4.67 4.84 5.01 5.18 5.36 5.53 5.70 5.87 6.05 6.22 6.39]-0.1;
bemf_v=[-0.16 0.13 0.37 0.56 0.73 0.87 0.94 0.98 0.99 1.00 1.00 0.99 0.98 ...
         0.96 0.90 0.78 0.61 0.43 0.20 -0.08 -0.33 -0.53 -0.70 -0.85 -0.94 ...
        -0.97 -0.99 -1.00 -1.00 -1.00 -0.98 -0.96 -0.91 -0.80 -0.64 -0.46 ...
        -0.25 0.03];
```

DEPARTMENT OF ELECTRICAL ENGINEERING
CHALMERS UNIVERSITY OF TECHNOLOGY
Gothenburg, Sweden
www.chalmers.se

CHALMERS
UNIVERSITY OF TECHNOLOGY